# A Sensor-less Flux-Switching Hybrid Excitation Generator using One Cycle Control

Zegang Xu [*,1], Shaojun Xie [2]

[1] *Department of Electrical Engineering,* Changzhou Institute of technology, Changzhou, 213032, China
[2] College of Automation Engineering, Nanjing University of Aeronautics and Astronautics, Nanjing 210016, China

***Abstract* — Flux-switching hybrid excitation machine (FSHM) is an interesting brushless machine with the advantage superiority of field adjustability. In this paper we address the challenges of rising costs and decreasing operational reliability by adding location sensors and employing one-cycle control (OCC) for FSHM generation system. Using field simulation and curve fitting, we establish FSHM model in Matlab/Simulink environment. To meet the requirements of OCC stability, armature current harmonic suppression and dynamic tracking performance, we consider the feasibility of using equivalent inductance as energy-storage inductance of PWM rectifier. The correctness and effectiveness of the proposed method are verified by simulation and experimental results on a 1.5kW prototype generator, which shows PWM rectifier adopting OCC strategy can effectively suppress the armature currents harmonics and keep the output DC voltage constant without position sensor.**

***Keywords - flux-switching machine; effective inductance; position-sensor less; PWM rectifier; one-cycle control***.

## . INTRODUCTION

The flux-switching hybrid excitation machines (FSHM) are of interest due to combining the advantages of simple and robust rotor structure, sinusoidal phase flux-linkage, and adjustable air-gap magnetic field[1-3]. In view of the fact that the bypass magnetic bridge(see Fig.1) not only maintains the stator lamination in its entireness, but also amplifies the effect of dc field windings on PM flux, the FSHM with an additional bridge has huge potential application in the wind turbines, avionic electric power system and vehicle power supply[4-7]. However, in order to balance the initial PM flux and flux control capability, the operating point of magnetic bridge at PM excitation should be chosen to the quasi-saturation region of magnetization curve, which may lead to the changing of dq-axis inductances[8].

Considering the FSHM phase flux linkage and phase back-electromotive force(EMF) are pure sinusoidal, space vector pulse width modulation(SVPWM) can be applied to improve power factor as well as dynamic performance, nevertheless, it is essentially not suitable for invariable $L_d$ and $L_q$[9]. The hysteresis current control method does not involve the variation of inductance parameter due to without calculating d-axis and q-axis voltage, whereas suffers from inconstant inverter switching frequency, which has a great impact on torque pulsation and harmonic content[10]. To achieve good performance while maintaining the advantage of having good tolerance for the inductance, an improved direct torque control(DTC) scheme using SVPWM, i.e., direct power angle linear control scheme is also investigated in [10].

The above mentioned SVPWM and DTC scheme require position information to meet the demand of control and monitoring, which increases the system cost and failure rate. Back electromotive force based methods (including model reference adaptive system, extended Kalman filter, sliding-mode observer, etc.) and signal injection methods for low speed range are attractive for position sensorless control applications, nevertheless, these methods have the shortcomings of depending on motor parameters, high frequency shiver, algorithm complexity, increase of power lose and torque ripple respectively[11-13].

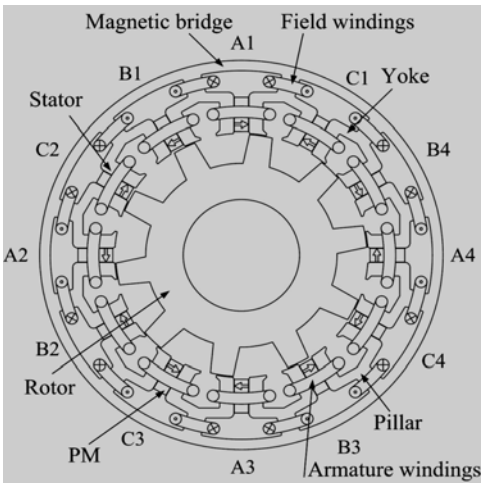

Fig. 1 Cross-section of 3-phase 12/10-pole FSHM..

This paper introduces one cycle control(OCC) applied in power factor corrected rectifiers into FSHM generation system to reduce total harmonic distortion. Simulation model is established based on the FSHM equivalent circuit according to 2D finite element analysis(FEA) in Section II. The operating principle of OCC-based three-phase converter is expounded in Section III. Detailed analytical studies are carried out to verify the feasibility of taking motor inductance as energy-storage inductance of PWM rectifier in Section IV. The viability of the scheme has been ascertained by MATLAB/SIMULINK calculations and measurements in Section V.

## Ⅱ .MODELING OF FSHM WITH MAGNETIC BRIDGE

### A. *Voltage Equation*

The flux linkage and back-EMF waveforms of FSHM machine with or without field excitation are close to sinusoidal distribution, indicates that the mathematical model of FSHM can be established in *dq* coordinates by applying the same methods used in synchronous machines. Furthermore, based on equivalent electrical circuit techniques, each phase of FSHM may be modeled as the generated voltage source(varying with rotor speed and excitation current) in series with the effective inductance (varying with core saturation) and armature resistance.

Due to symmetry, three-phase inductors have the same values, namely $L_a$=$L_b$=$L_c$=$L_s$, and voltage equation can be expressed as:

$$\begin{cases} u_a = \omega_e(L_{ev}I_f + \psi_{m0})\sin(\omega_e t) + L_s p i_a + R_s i_a \\ u_b = \omega_e(L_{ev}I_f + \psi_{m0})\sin(\omega_e t - 2\pi/3) + L_s p i_b + R_s i_b \\ u_c = \omega_e(L_{ev}I_f + \psi_{m0})\sin(\omega_e t + 2\pi/3) + L_s p i_c + R_s i_c \end{cases} \quad (1)$$

where $p$ is differential operator, $I_f$ is field current, $\omega_e$ is the rotor electrical angular speed, $R_s$ is armature resistance, $\psi_{m0}$ is the maximum no-load flux without field excitation, and $L_{ev}$ is the mutual inductance between armature winding and field winding.

### B. *Inductances calculating and fitting*

According to (1), the key of model building lies in the inductances calculating and curve fitting. When a specific $I_f$ is injected into excitation winding, both the PM excitation and the electric excitation take effect simultaneously, thus the relationship between $L_{ev}$ and $I_f$ is expressed as

$$L_{ev} = (\psi_{hy} - \psi_{m0})/I_f \quad (2)$$

where, $\psi_{hy}$ is synthesis flux linkage with hybrid excitation. Obviously, FEA simulation will cost too much effort and computing time to repeat in the range of positive and negative rated field current(±5A) with a small step size, in addition, for continuous system simulation, time-consuming problem also exists in interpolation operation. On account of this, a simplified and fast approach is performed based on two steps. Firstly, as shown in Fig.2, the forecasting values are obtained by MATLAB Spline function based on sample data with the step of 1A. Whilst, a higher order polynomial, given as (3), is adopted to fit the output data from Spline model with the maximum relative error of 3.1%.

$$\begin{aligned} L_{ev} = {} & 2.65\times10^{-5}I_f^8 - 2.11\times10^{-4}I_f^7 - 2.72\times10^{-3}I_f^6 \\ & + 4.52\times10^{-3}I_f^5 + 6.65\times10^{-2}I_f^4 + 4.92\times10^{-2}I_f^3 \\ & - 1.96\times10^{-1}I_f^2 + 9.84\times10^{-1}I_f + 12.7 \ \ (mH) \end{aligned} \quad (3)$$

When FSHM generator runs with three-phase pure resistive load, effective inductance satisfies:

$$L_s = \frac{\sqrt{R_l^2E_0^2 - U_s^2(R_l + R_s)^2}}{2\pi N_r n_r U_s / 60} \quad (4)$$

where $R_l$ is load resistance, $N_r$ is the rotor pole number, $n_r$ is the rated speed, $E_0$ and $U_s$ are, respectively, no-load voltage and load side voltage.

Since $L_s$ involves the two-variate function of field current and armature current due to magnetic saturation, it is necessary to investigate the change law of $L_s$ on the basis of load characteristics with different $I_f$. As a result, a three-dimensional nonlinear inductance with the range of 1.2-fold of rated current is given in Fig. 2.

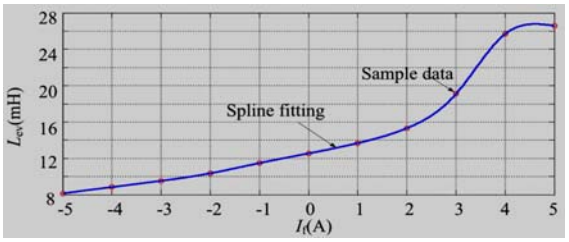


Fig. 2 $L_{ev}$ with varying field current.

Surface approximating method using bicubic polynomials is a evolution from least square curve fitting method. It is noted that, the increasing of the order of interpolation will lead to Runge phenomena, which has negative implication on computational instability. In terms of obvious difference in fluctuation trend on each side of $I_f$ =2A(as shown in Fig.3), piecewise fitting is an efficient way, from this, a two dimensional curve is described as 3-order polynomial ($I_f$ <2A), whereas a tridimensional curved surface is described as bicubic polynomials ($I_f$≥2A), and then, corresponding formula is given as:

$$L_s = \begin{cases} 3.92\times10^{-6}I_f^3 + 8.81\times10^{-5}I_f^2 + 1.14\times10^{-3}I_f + 1.55\times10^{-2} & (<2A) \\ \begin{bmatrix} 6.10\times10^{-5} & -5.92\times10^{-4} & 1.78\times10^{-3} & -1.64\times10^{-3} \\ -5.26\times10^{-4} & 5.33\times10^{-3} & -1.67\times10^{-2} & 1.61\times10^{-2} \\ 4.89\times10^{-4} & -4.92\times10^{-3} & 1.55\times10^{-2} & -1.54\times10^{-2} \\ -5.78\times10^{-4} & 2.55\times10^{-3} & 3.61\times10^{-3} & 6.18\times10^{-3} \end{bmatrix} \begin{bmatrix} I_f^3 \\ I_f^2 \\ I_f^1 \\ I_f^0 \end{bmatrix} \begin{bmatrix} I_s^3 \\ I_s^2 \\ I_s^1 \\ I_s^0 \end{bmatrix} & (\geq 2A) \end{cases} \quad (5)$$

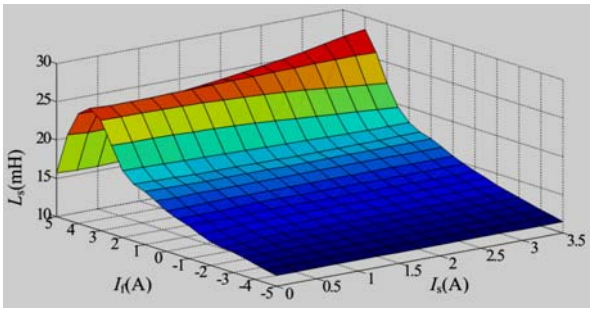


Fig.3 The change law of $L_s$.

## Ⅲ. PRINCIPLE AND IMPLEMENTATION OF OCC CONTROLLED AC/DC CONVERTER

Fig.4 shows the schematic of PWM rectifier with one cycle control. The rectifier is composed of six switches in a three-phase bridge, which is directly connected to the output end of the FSHM generator, and the dc-bus capacitor $C_{dc}$ at the other side, which acts as an energy storage unit for the load.

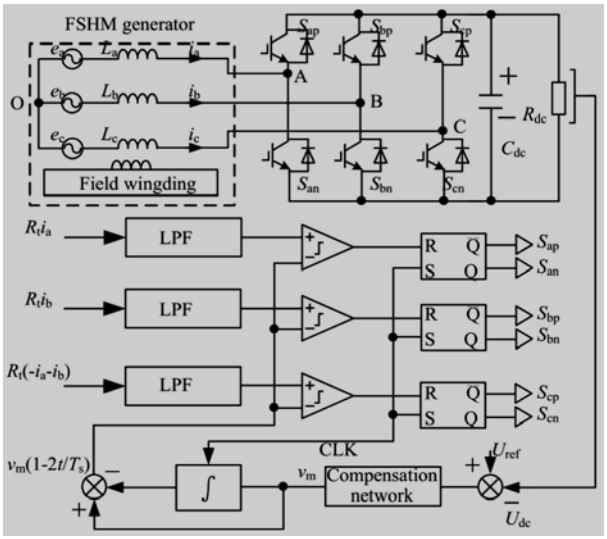


Fig. 4 Schematic of FSHM PWM rectifier with one cycle control.

Assuming the average voltage across the effective inductance in a switching period to be zero by means of "voltage-second" balance principle, the average voltages $u_{jO}(j=a,b,c)$ respecting to node O satisfy:

$$\begin{cases} u_{AO} \approx e_a = E_m \sin(\omega_l t) \\ u_{BO} \approx e_b = E_m \sin(\omega_l t - 2\pi/3) \\ u_{CO} \approx e_c = E_m \sin(\omega_l t + 2\pi/3) \end{cases} \tag{6}$$

where $e_j(j=a,b,c)$, $E_m$ are respectively, three-phase back-EMFs and the corresponding amplitude.

In order to have unity power factor, the armature currents should follow the three-phase sinusoidal back-EMFs. Define $R_e$ as the emulated resistance looking from motor side, the relationship between the input voltages and currents can be expressed as:

$$e_j = R_e i_j \quad (j = a,b,c) \tag{7}$$

Combination (6) and (7), the kernel control equations can be derived as following[14]

$$R_t i_j = v_m(1-2d_{jn}) \quad (j = a,b,c) \tag{8}$$

where $R_t$ is test resistance for sampling armature current, $d_{jn}(j=a,b,c)$ represent duty ratios for three phase lower switches, and $v_m$ is the output of the feedback error compensator. While set the time constant of the integrator $T_i=T_s/2$, where $T_s$ is switching period, $v_m$ is defined as $U_{dc}R_t/(2R_e)$.

According to (8), the turn-on instant of three phase lower switches can be achieved by Ramp comparison, which compares the sampling current (modified by a low-pass filter, LPF) with the saw-tooth waveform (generated by the resettable integral of $v_m$), and then the turn-off instant of higher switches can be determined by taking complementary control strategies in each arm. Apparently, OCC strategy used in the power factor correction(PFC) has the merit of constant switching frequency, and no need for sampling input phase and frequency.

## Ⅳ. FEASIBLE ANALYSIS OF USING MOTOR INDUCTANCE AS ENERGY STORGE INDUCTANCE

### A. OCC Stability

For the operating waveforms with peak armature current sensing, as given Fig.5, the stable operation condition with one cycle control is[15]:

$$\left|\frac{m_c - m_2}{m_c + m_1}\right| \le 1 \tag{9}$$

where the rising slop $m_1=R_tv_a/L_a$, the falling slop of rising edge $m_2=R_t(U_{dc}-v_a)/L_a$, and effective slop the saw-tooth carrier $m_c=2v_m/T_s=R_tU_{dc}/(R_eT_s)$.

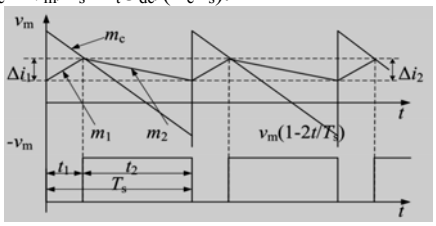


Fig. 5 Operating waveforms with peak armature current sensing.

This leads to

$$v_m \ge U_{dc}R_tT_s/(4L_a) \tag{10}$$

Combining the definition of $v_m$ and $R_e=1.5E_{m2}/P_2$, where $P_2$ is the nominal power output, yields:

$$L_a \ge 3E_m^2T_s/(4P_2) \tag{11}$$

### B. Armature Current Ripple

As shown in Fig.4, the A phase voltage equation is given by

$$L_a\frac{di_a}{dt} = e_a + \frac{-2S_{ap}+S_{bp}+S_{cp}}{3}U_{dc} \tag{12}$$

where $S_{jp}$($j$=$a,b,c$) are switching functions of three phase higher switches. For $S_{ap}$=0 and $S_{ap}$=1 instant, exists

$$L_a\frac{\Delta i_1}{t_1}=e_a+\frac{S_{bp}+S_{cp}}{3}U_{dc}\qquad(S_{ap}=0) \tag{13}$$

$$L_a\frac{\Delta i_2}{t_2}=e_a+\frac{S_{bp}+S_{cp}-2}{3}U_{dc}\quad(S_{ap}=1) \tag{14}$$

As the load reaches the peak, $e_a$ is approximately equal to $E_m$, and the current variation during turn-on and turn-off instant have the same value. Considering the boost characteristic of PFC circuits(DC bus voltage having a higher level than that of peak line-to-line), and the limiting condition for each switch ($S_{bp}$=$S_{cp}$=0), the lower limit for effective inductance can be carried out:

$$L_a\geq\frac{(2U_{dc}-3E_m)E_mT_s}{2U_{dc}\Delta i_{am}} \tag{15}$$

Furthermore, assuming that the maximum ripple is less than 20% peak current $I_m$, where $I_m$=$2P_2$/(3$E_m$), equation (15) can be rewritten as:

$$L_a\geq\frac{3E_m^2T_s(2U_{dc}-3E_m)}{0.8U_{dc}P_2} \tag{16}$$

### C. Dynamic Tracking Performance

Although previous derivation provide some reference for lower limit, there is a upper one to the energy-storage inductance in terms of dynamic tracking performance. Noted that the maximum of current rate appears near zero-cross point, thereout, operating waveforms during current reversal are given in Fig.6.

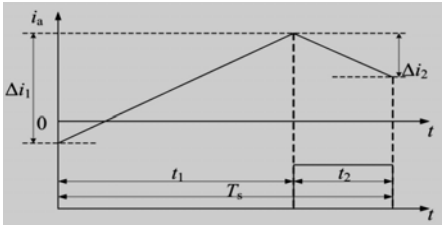


Fig. 6 Operating waveforms during current reversal.

Using an acceptable approximation of $e_a$=0 at current zero, and taking a similar approach used in the analysis of armature current ripple, the following equation can be obtained

$$\frac{|\Delta i_1|-|\Delta i_2|}{T_s}\geq\frac{I_m\sin\omega T_s}{T_s}\approx\omega I_m \tag{17}$$

In view of the switching limiting condition($S_{bp}$=$S_{cp}$=1), and maximum-slope occurring with $t_1\rightarrow T_s$, it yields

$$L_a\leq 2U_{dc}/(3\omega I_m) \tag{18}$$

Moreover, the maximum no-load back-EMF $E_m$ satisfies:

$$E_m=\omega N_{ph}\phi_{gA} \tag{19}$$

Substituting the expression of $I_m$ and (19) into (18) and rearranging slightly, then gives the following expression for the upper limit

$$L_a\leq U_{dc}N_{ph}\phi_{gA}/P_2 \tag{20}$$

where, $\Phi_{gA}$ is peak flux, and $N_{ph}$ is number of turns per phase.

### D. Calculation examples

The major design parameters of the 12/10 pole FSHM power system are given in appendix, according to the FEA simulation results, the corresponding $E_m$(field-enhancing +1200A•T) and $\Phi_{gA}$ (field-weakening -1200A•T) are 311V and 0.345mWb respectively. Fig. 7 presents the comparison of the value range of energy storage inductances and the effective inductance at rated armature current.

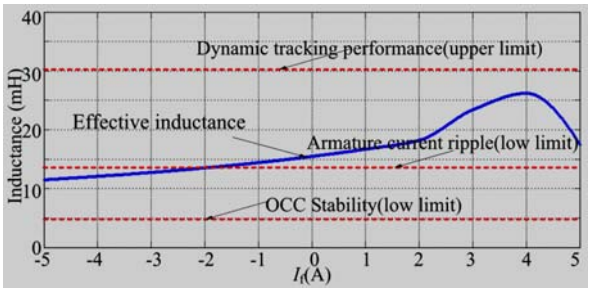


Fig. 7 Value range of energy storage inductances and effective inductance.

It can be found that effective inductance always meets the design requirement for dynamic tracking performance and OCC stability, whereas shows a little below that for armature current ripple when the filed current is less than -2A. By the way, taking the influence of end-effect into account, the actual value of effective inductance should be slightly above the 2-D predicted result, which confirms that the current ripple can be held to the desired level.

## □. EXPERIMENTAL VALIDATION

Taking the A phase FSHM for example, the simulation model based on Matlab/Simulink is shown in Fig.8. $L_{ev}$ and $L_s$ in different conditions can be obtained by fitting functions, which avoids the time-consuming transient co-simulation [16], so that the performance analysis will become more efficient.

In Fig.9 and Fig.10, the waveforms of armature current and dc-bus voltage($n_r$=1200r/min, $I_f$=5A, $R_{dc}$=350Ω, and $n_r$=800r/m, $I_f$=0A, $R_{dc}$=2kΩ) evaluated by Matlab/Simulink model are compared with experimental results respectively, which are in good agreement in both magnitudes and shapes. As can be noted from the plots, the phase current waveforms are approximately close to sinusoidal distribution under different rectifier loads(about 80% and 15% of rated load) and varying frequency($f$=$N_r n_r$/60) while that the DC output voltages keep around the predetermined value(650V).

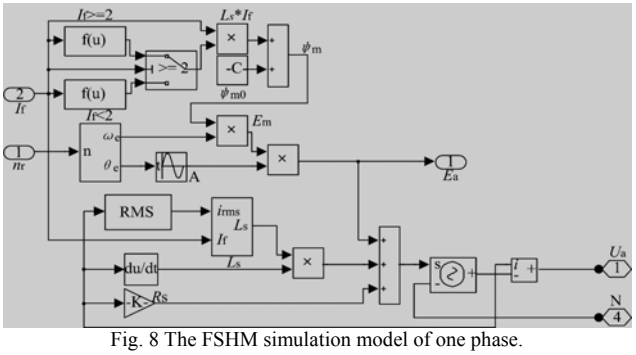


Fig. 8 The FSHM simulation model of one phase.

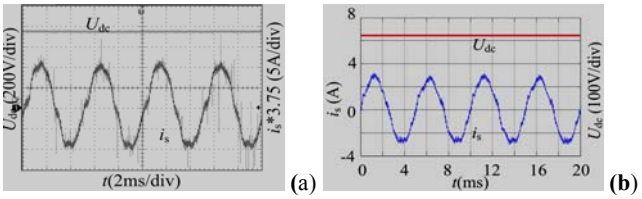


Fig. 9 Phase current and dc voltage at 1200 r/min, $I_f$=5A, $R_{dc}$=350Ω.
(a) Measured. (b) Simulated.

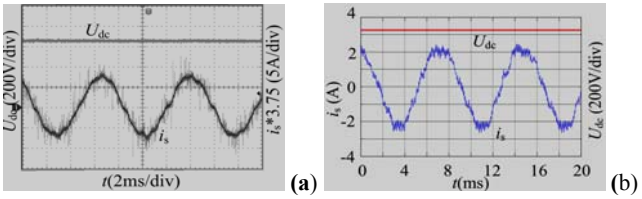


Fig. 10 Phase current and dc voltage at $n_r$=800r/m, $I_f$=0A, $R_{dc}$=2kΩ.
(a) Measured. (b) Simulated.

Furthermore, Fig.11 presents the predicted and measured spectrum analysis for armature current in Fig.9. It can be observed that the harmonic components have been suppressed to a very low degree, among them, the lowest harmonic component is 4.2% of fundamental current.

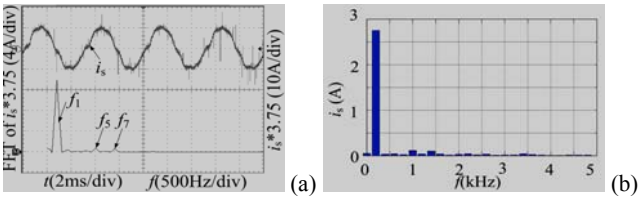


Fig.11 Spectrum analysis for armature current in Fig.9.
(a) Measured. (b) Simulated.

## . CONCLUSIONS

In this paper, according to the inductances analysis and modeling of flux-switching hybrid excitation machine with magnetic bridge, a new implementation scheme using OCC controller is employed for brushless DC generator system. The proposed scheme adopts the effective inductance of the motor as energy-storage inductance, and no position sensors are used. Simulation and experimental results haven proven that harmonic contents can be reduced significantly under the PWM modulation, which also offers an alternative position sensorless control for sine wave synchronous motor.

The future work includes:

(a) The current phase lag issue of OCC PFC converter, especially in inductance nonlinearity caused by field saturation.

(b) Coordinated control of rectifier duty ratio and field current, using minimum copper and core losses as optimization target.

## APPENDIX

### DESIGN PARAMETERS OF 12/10 POLE FSHM POWER SYSTEM

| | | | |
|---|---|---|---|
| Outer stator diameter (mm) | 155 | Number of turns per phase | 256 |
| Inner stator diameter (mm) | 98 | Magnet dimensions ($mm^3$) | 5.5×13.5×98 |
| Active axial length (mm) | 98 | Magnet remanence (T) | 1.2 |
| Air-gap length (mm) | 0.3 | Stator tooth arc factor | 0.25 |
| Stator yoke thickness (mm) | 4.0 | Rated speed (rpm) | 1200 |
| Iron bridge thickness (mm) | 3.5 | Field turns (T) | 240 |
| Iron bridge pillar width (mm) | 7.0 | Rotor pole-arc angle (°) | 15 |
| Nominal power output (kW) | 1.5 | Dc-bus voltage (V) | 650 |
| Switching frequency (kHz) | 10 | Filter capacitor (mF) | 1 |

## CONFLICT OF INTEREST

The author confirms that this article content has no conflict of interest.

## ACKNOWLEDGEMENTS

This work was supported by 333 High Level Valuation Professional Training of Jiangsu province China and Top-notch Academic Programs Project High Education Institution (TAPP).

## REFERENCES

[1] W. Hua, M. Cheng, G. Zhang, "A novel hybrid excitation flux-switching motor for hybrid vehicles", *IEEE Transactions on Magnetics*, vol. 45, no. 10, pp.4728-4731,2009.

[2] E. Sulaiman, T. Kosaka, N. Matsui, "A novel hybrid excitation flux switching synchronous machine for a high-speed hybrid electric vehicle applications", *International Conference on Electrical Machines and Systems*, Beijing , 2011, pp. 1-6.

[3] J. S. Jang, J. K. Lee, B. T. Kim, "Characteristic analysis of a hybrid excited flux switching PM motor by using the equivalent magnetic circuit method", International Journal of Applied Electromagnetics and Mechanics, vol. 39, pp. 843-849, 2012.

[4] E. Hoang, M. Lecrivain, M. Gabsi, "A new structure of a switching flux synchronous polyphased machine with hybrid excitation", *European Conference on Power Electronics and Applications*, Aalborg, Denmark, 2007, pp. 1-8.

[5] R. L. Owen, Z. Q. Zhu, G. W. Jewell, "Hybrid-excited flux-switching permanent-magnet machines with iron flux bridges", *IEEE Transactions on Magnetics*, vol. 46, no. 6, pp. 1726-1729, 2010.

[6] E. Sulaiman, T. Kosaka, Y Tsujimori, et al, "Design of 12-slot 10-pole permanent magnet flux-switching machine with hybrid excitation for hybrid electric vehicle", *5th IET International Conference on vehicle Power Electronics*, *Machines and Drives*, Brighton, United Kingdom, 2010, pp.1-5.

[7] E. Sulaiman, T. Kosaka, N Matsui, "High power density design of 6-Slot 8-Pole hybrid excitation flux switching machine for hybrid electric vehicles", *IEEE Transactions on Magnetics*, vol. 47, no. 10, pp. 4453-4456, 2011.

[8] Z. G. Xu, S. J. Xie, P. Mao, "Analytical design of flux-switching hybrid excitation machine by a nonlinear magnetic circuit method. I*EEE Transactions on Magnetics*, vol.49,no.6, pp. 3002-3008, 2013.

[9] Y. Zhu, M. Cheng, W. Hua, et al. "V Space-vector PWM control of flux-switching permanent magnet motor", *Electric Machines and Control*, vol. 14, no. 3, pp. 45-50, 2010.

[10] Y. Wang, Z. Q. Deng, "Analysis of electromagnetic performance and control schemes of electrical excitation flux-switching machine for DC power systems", *IEEE Transactions on energy conversion*, vol. 27, no. 4, pp. 844-855, 2012.

[11] Y. Wang, Z. Q. Deng, "A position sensorless method for direct torque control with space vector modulation of hybrid excitation flux-switching generator", *IEEE Transactions on Energy Conversion*, vol. 27, no. 4, pp. 912-921, 2012.

[12] W. Qiao, X. Yang, X. Gong, "Wind speed and rotor position sensorless control for direct-drive PMG wind turbines", *IEEE Transactions on Industry Applications*, vol. 48, no. 1, pp. 3-11, 2012.

[13] Y. C. Shi, K. Sun, L. P. Huang, et al, "Online identification of permanent magnet flux based on extended Kalman filter for IPMSM drive with position sensorless control", *IEEE Transactions on Industry Electronics*, vol. 59, no. 11, pp. 4069-4178, 2012.

[14] C. M. Qiao, K. M. Smedley, "Unified constant-frequency integration control of three-phase standard bridge boost rectifiers with power-factor correction", *IEEE Transactions on Industrial Electronics*, vol. 50, no. 1, pp. 100-107, 2003.

[15] G. Z. Chen, K. M. Smedley, "Steady-state and dynamic study of one-cycle-controlled three-phase power-factor correction", *IEEE Transactions on Industrial Electronics*, vol. 52, no. 2, pp. 355-362, 2005.

[16] X. Y. Zhu, M. Cheng, W. X. Zhao, et al, "A transient cosimulation approach to performance analysis of hybrid excited doubly salient machine considering indirect field-circuit coupling", IEEE Transactions on Magnetics, vol. 43, no. 6, pp. 2558-2650, 2007.